Ce^{3+} Ions Determine Redox-Dependent Anti-apoptotic Effect of Cerium Oxide Nanoparticles

Ivana Celardo,[†] Milena De Nicola,[†] Corrado Mandoli,[‡] Jens Z. Pedersen,[†] Enrico Traversa,[‡,*] and Lina Ghibelli[†,*]

[†]Department of Biology, University of Roma "Tor Vergata", Rome, Italy and [‡]International Research Center for Materials Nanoarchitectonics (MANA), National Institute for Materials Science (NIMS), Tsukuba, Japan.

ABSTRACT Antioxidant therapy is the novel frontier to prevent and treat an impressive series of severe human diseases, and the search for adequate antioxidant drugs is fervent. Cerium oxide nanoparticles (nanoceria) are redox-active owing to the coexistence of Ce^{3+} and Ce^{4+} oxidation states and to the fact that Ce^{3+} defects, and the compensating oxygen vacancies, are more abundant at the surface. Nanoceria particles exert outstanding antioxidant effects *in vivo* acting as well-tolerated anti-age and anti-inflammatory agents, potentially being innovative therapeutic tools. However, the biological antioxidant mechanisms are still unclear. Here, the analysis on two leukocyte cell lines undergoing apoptosis *via* redox-dependent or independent mechanisms revealed that the intracellular antioxidant effect is the direct cause of the anti-apoptotic and prosurvival effects of nanoceria. Doping with increasing concentrations of Sm^{3+}, which progressively decreased Ce^{3+} without affecting oxygen vacancies, blunted these effects, demonstrating that Ce^{3+}/Ce^{4+} redox reactions are responsible for the outstanding biological properties of nanoceria.

KEYWORDS: cerium oxide · nanoparticles · antioxidant effect · apoptosis · leukocytes

The etiology or development of many serious diseases involves oxidative stress, a condition where the reactive oxygen species (ROS) produced by the aerobic metabolism are insufficiently buffered by cell or tissue antioxidant defenses.[1] The excess of ROS damages DNA, proteins, and lipids, leading to cell malfunction or death and to tissue damage,[2] and contributing to pathologies such as cancer, immuno-deficiencies, neurodegenerative disorders, early aging, viral pathogenesis, diabetes, ischemia, sepsis, chronic inflammation, and many others.[3,4] For this reason, in the last two decades, antioxidant therapy is the focus of enormous clinical interest,[5] and great emphasis is given to nutritional and pharmacological strategies to prevent or ameliorate human diseases by supplementing antioxidant molecules that enhance or mimic endogenous antiradical defenses.[6,7] In fact, the ideal antioxidant therapy is still elusive because of many intrinsic variables, such as the choice of the adequate antioxidant system and the correct dosage; excess of ROS scavenging would be deleterious because basal ROS are required for correct cell and tissue functioning.[8]

Great expectations derive from nanotechnology approaches, including redox-active metal oxide nanoparticles, such as nanoceria. In CeO_2, a fraction of Ce is in the Ce^{3+} form; the reduction in positive charge is compensated by a corresponding number of oxygen vacancies. These defects are enriched at the surface;[9,10] therefore, nanoceria has a relatively larger Ce^{3+} content with respect to micrometer-sized counterparts, owing to the increase in the surface-to-volume ratio.[11,12] The coexistence of Ce^{3+} and Ce^{4+} ions produces redox reactions, resulting in catalytic activity[13,14] that makes nanoceria suitable for numerous industrial applications, including catalysis,[15] solid oxide fuel cells,[16,17] solar cells,[18] gas sensors,[19] and solar fuel production.[20] These redox properties have attracted the interest of the scientific community for the potential exploitation of nanoceria as antioxidant in biological systems.[21−23] An open problem is decoupling the influence of the surface defects on the nanoceria antioxidant mechanisms. On one side, oxygen vacancies may allocate oxygen moieties of biological molecules, inhibiting a set of pro-oxidant biological effects. On the other side, the Ce^{3+}/Ce^{4+} cycles allow nanoceria to react catalytically with superoxide and hydrogen peroxide, mimicking the action of two key antioxidant enzymes, superoxide dismutase (SOD) and catalase.[24] Since SOD and catalase mimesis are performed by oxidation of Ce^{3+}[24] and reduction of Ce^{4+},[25] respectively, the coexistence of H_2O_2 and superoxide in cells renders nanoceria a potential self-regenerating biological antioxidant.[26]

* Address correspondence to ghibelli@uniroma2.it, traversa.enrico@nims.go.jp.

Received for review January 13, 2011 and accepted May 26, 2011.

Published online May 26, 2011
10.1021/nn200126a

Initial studies have shown that nanoceria is well-tolerated by the organism,[27] has anti-inflammatory properties,[28] and is neuro-[29] and cardioprotective.[30] At the cellular level, it generally exerts prosurvival and antiradical effects.[31,32] It remains to be investigated whether these phenomena are linked by a cause–effect relationship, which is conceivable, since apoptosis partially depends on oxidation. Apoptosis is a homeostatic mechanism of cell suicide of supernumerary, senescent, or damaged cells, occurring through sophisticated signal transduction pathways and leading to gentle cell elimination.[33] Damage by oxidative stress can trigger apoptosis;[34] accordingly, oxidative pathologies imply increased apoptosis and loss of tissue function, particularly severe in poorly renewable tissues such as brain or in regulative compartments such as leukocytes in inflammation.[35]

Here, we investigate the antioxidant mechanism of nanoceria in two leukocyte cell lines, each undergoing apoptosis *via* either redox-dependent or independent pathways. We demonstrate for the first time, to the best of our knowledge, a direct cause–effect relationship between the cell antiradical and prosurvival effects of nanoceria. Moreover, tailoring nanoceria with different levels of Sm doping, which decreases Ce^{3+} without affecting oxygen vacancy contents, we demonstrate that Ce^{3+}/Ce^{4+} redox reactions are responsible for the outstanding biological properties of nanoceria.

RESULTS AND DISCUSSION

Nanoceria in Aqueous Suspension. The nanoceria used in this study was synthesized using a wet-chemical route,[36] which allows obtaining nanocrystalline ceria at room temperature; organic residues were removed by heating to 450 °C,[17] and powders prepared at this temperature were used in this work for the biological analyses. Particle size measured using transmission electron microscopy (TEM) observations is in the 5–16 nm range; the BET specific surface area was measured at 57 $m^2\ g^{-1}$ (see previous papers for further characterization[17,36]).

Pristine nanoceria particles tend to form aggregates, especially after suspension in aqueous solution, dramatically reducing the active surface and possibly impairing bioactivity. Figure 1A shows light micrographs of different concentrations of nanoceria suspensions as they appear when placed in contact with U937 cells; the agglomerates are easily detectable (see arrows in the figure), increasing in number and size with increasing the nanoceria concentration (CTRL = no nanoceria; 20, 100, and 200 μg/mL), and are randomly distributed, suggesting the absence of specific interactions with the cells. At such magnification, the separated nanoparticles are not visible, nor it is possible to detect an eventual intracellular localization. To assess nanoceria internalization, we performed a flow cytometric analysis of side scatter, a parameter that measures intracellular dis-homogeneity. It was recently shown that nanoparticle internalization, as detected by TEM analysis, leads to (and strictly correlates with) an increase in cell side scatter, and that internalization mostly depends on the type of particles; for example, nanotitania was among the particles that were most efficiently internalized, whereas nanoceria was not included in the analysis.[37] Therefore, we used as a positive control nanotitania (anatase) powder with similar size and physicochemical characteristics as nanoceria, already used as a control for nanoceria activity in a previous work.[36] We observed that nanotitania, but not nanoceria, affected cell side scatter, which is evidenced by the upward smear in the second dot plot of Figure 1B (arrow), implying no or negligible internalization of our nanoceria preparations. This different behavior, which can be hardly attributed to the similar physicochemical characteristics for both nanoparticles, is presently under investigation.

Aggregation can be prevented by capping with surfactants or organic molecules;[38] however, these treatments may also alter the native properties of nanoceria, whose analysis is the scope of this study. Therefore, we decided to avoid such modifications. The use of pristine nanoceria required quantifying and characterizing the fraction of bioactive nanoparticles left after aggregation. To this purpose, nanoceria suspensions were let to sediment overnight in distilled water; colloidal nanoparticles remaining in the supernatant were separated from the larger aggregates in the settled cake. When the supernatant fraction was added to the cells, no agglomerates were detectable (Figure 1A "super"). The supernatant was dried to collect the ultrafine powder, which was weighed out, showing that about 10 wt % of nanoceria remained in this fraction. The morphology of the nanoceria particles obtained from the supernatant was observed using TEM. Figure 1 shows the typical bright field TEM micrographs at low (Figure 1C) and high (Figure 1D) magnifications. The powder consisted of agglomerated polyhedral particles, characterized by low-dimensional dispersion and mean size ranging from 5 to 8 nm. The related electron diffraction pattern (inset in Figure 1C) shows reflection lines compatible with CeO_2 having fluorite structure (PDF-ICDD card #34-0394, JCPDS International Center for Diffraction Data, 2000). The high-resolution micrograph (Figure 1D) shows clear lattice fringes with *d* spacing of 3 Å (white lines in Figure 1D), which correspond to the distance between the (111) lattice planes of ceria. Overall, the sedimentation procedure in water eliminated the original aggregates and the larger primary particles (class 9–16 nm), as resulting from the measurement of size distribution before and after sedimentation (Figure 1E); this is compatible with aggregation of particles large enough to lack

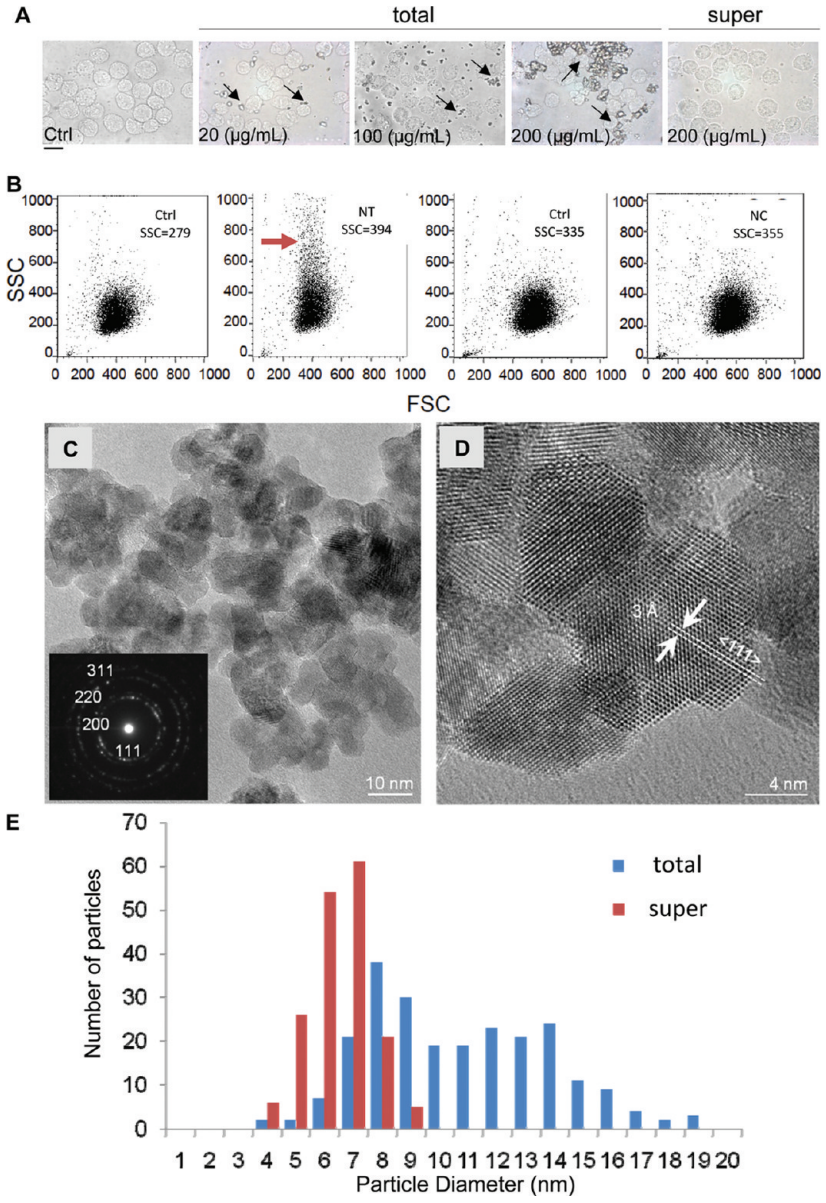

Figure 1. Morphological analysis of the CeO_2 powder and suspensions. (A) Phase contrast microscopy images of U937 cells alone (CTRL) or incubated for 24 h in the presence/absence of increasing concentrations of total nanoceria (20, 100, and 200 μg/mL) or the supernatant (super) fraction from 200 μg/mL, separated as described in the text. Black arrows indicate nanoceria precipitated; bar = 20 μm. (B) Flow cytometric analysis of forward (FSC) *vs* side (SSC) scatter of U937 cells incubated for 2.5 h with 100 μg/mL nanoceria (NC, right) or 100 μg/mL nanotitania (NT, left), each with its control of untreated cells. The mean values of SSC for each treatment are shown. Only nanotitania produces an upward smear (arrow); one of >10 experiments is shown; similar analyses on Jurkat cells gave similar results. (C) Bright field TEM image of the ceria nanoparticles at lower magnification, and (inset) indexed electron diffraction pattern in the reciprocal space. (D) High-resolution TEM image showing lattice fringes and *d* spacing related to the (111) crystalline planes. (E) Particle size distribution in the total or supernatant fraction of nanoceria, obtained from analysis of the HR-TEM micrographs. The diameter of $n > 150$ randomly selected nanoparticles from each sample was measured; values are reported as number of particles belonging to different class sizes.

surface charge and undergo aggregation and precipitation.

Nanoceria as Potent Antioxidant. The antioxidant effect of the pristine nanoceria preparations was analyzed with *in vitro* tests, which demonstrated that 200 μg/mL of nanoceria potently reduced the stable radical galvinoxyl[39] (Figure 2A). Next, we separately tested the supernatant *versus* sediment fraction. The supernatant retained all of the antioxidant activity, as shown by the linear dose–response obtained by incubating galvinoxyl with increasing amount of supernatant fraction (Figure 2B,C), whereas the sediment fraction showed no detectable activity independently of the amount of sample added (Figure 2C).

For the studies on cells, we chose two established leukocytic cell lines, namely, the human tumor monocytes U937, our leading model, and the human tumor T lymphocytes Jurkat, which are suitable, complementary

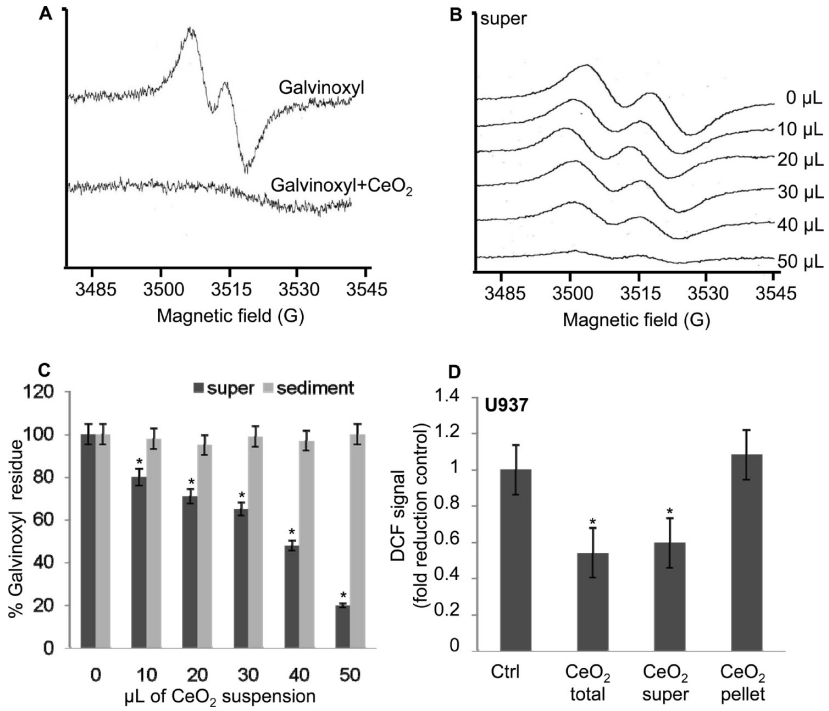

Figure 2. Antiradical effect of nanoceria is limited to the supernatant fraction. (A) EPR spectra showing galvinoxyl (10 μM) reduction by 200 μg/mL nanoceria at 2 h incubation. Nanoceria at these conditions eliminates galvinoxyl signal (100% loss) in 4/4 independent experiments performed. (B) EPR profiles of galvinoxyl (100 μM) after 2 h incubation with increasing amount of the supernatant (super) fractions of nanoceria obtained after sedimentation from a 10 mg/mL suspension as described in Materials and Methods. (C) Quantification of the residual galvinoxyl signal after incubation with increasing amounts of the supernatant (dark bars) or sediment (light bars) fractions of nanoceria. Values represent the mean of four independent experiments $\pm$ SD; *$p < 0.05$ compared to the control. (D) Intracellular ROS at 24 h incubation with total nanoceria (200 μg/mL), with the supernatant fraction after overnight sedimentation, and with the sediment fraction, as described in Materials and Methods. Values indicate fold increase with respect to control and represent the mean of four independent experiments $\pm$ SD; *$p < 0.05$ compared to the control.

models of inflammatory cells, extremely well investigated in terms of redox metabolism and apoptosis.

The effect of nanoceria on the basal intracellular redox state of U937 cells was then investigated, evaluating intracellular ROS levels by flow cytometric analysis of dichlorofluorescein (DCF) stained cells. Nanoceria is a potent antioxidant also in cells, and also in this case, the supernatant fraction retained all of the antioxidant activity, whereas none was detected in the sediment fraction (Figure 2D). Considering that the active fraction is about 10% of the total mass, this finding allows determining that the nominal 200 μg/mL concentration is in fact an active concentration of about 20 μg/mL. This conclusion can be drawn since all of the physicochemical characteristics measured for the pristine powder and the supernatant fraction were the same, apart from the particle size and associated parameters. For uniformity with previous work, all of the experiments of the present study were performed with total (*i.e.*, without separation by sedimentation) nanoceria preparations, except when stated.

We characterized the intracellular antioxidant activity of nanoceria. Within the nominal 5−200 μg/mL concentration range, nanoceria dose-dependently reduced basal ROS levels after 6 h (Figure 3A). A time course with the 200 μg/mL concentration shows that nanoceria reduced ROS in a time-dependent fashion in U937 (Figure 3B) and Jurkat cells (Figure 3C), progressively decreasing ROS levels, even at time points as late as 48 and 72 h; this is a very peculiar effect that was not observed with other widely used intracellular antioxidants (Figure 3D).

Nanoceria Decreases Damage-Induced Apoptosis. The effects of nanoceria on cell viability were then analyzed. Nanoceria did not exert any cytotoxic effect in our cell systems for up to 72 h, as shown by cell count, MTT assay, and extent of basal apoptosis or necrosis. We next investigated whether nanoceria could protect against cell apoptosis. Apoptosis was induced by three different cell-damaging agents that elicit the intrinsic apoptotic pathway, namely, hydrogen peroxide, the protein synthesis inhibitor puromycin (PMC), and the topoisomerase II inhibitor etoposide (VP-16); these agents induce apoptosis by different kinetics and mechanisms, which were thoroughly analyzed in previous studies.[40,41] Figure 4A shows that nanoceria dose-dependently decreases the extent of apoptosis induced in U937 by the three agents, measured as the fraction of apoptotic nuclei; micrographs of Hoechst-stained control and VP-16-treated U937 are shown in

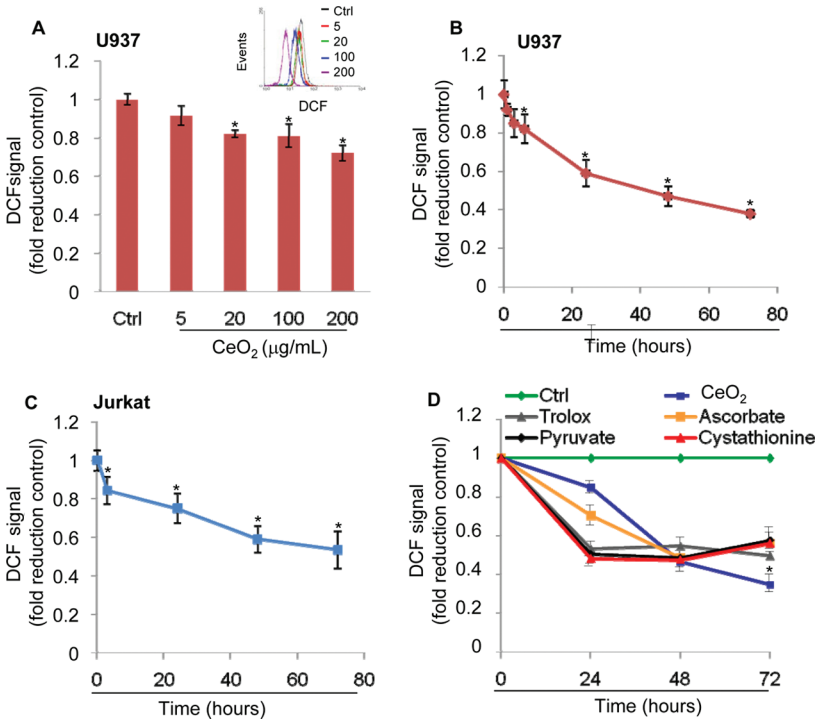

Figure 3. Nanoceria reduces intracellular free radicals. (A) Intracellular ROS measured as DCF signal by flow cytometry at 6 h exposure to nanoceria (5, 20, 100, and 200 μg/mL); data represent the mean of four independent experiments $\pm$ SD and are provided as % reduction with respect to control; the inset shows the overlay of the flow cytometric profiles of cells treated with the various nanoceria concentrations as indicated by the numbers in the legend; *$p < 0.05$ compared to the control. Time course analysis of intracellular ROS levels on (B) U937 and (C) Jurkat cells upon incubation with 200 μg/mL nanoceria; data represent the fold reduction of the DCF signal with respect to control and are the mean of four independent experiments $\pm$ SD; *$p < 0.05$ compared to the control. (D) Comparison of different antioxidant treatments. U937 cells were incubated at 37 °C with 1 mM trolox, 100 μM sodium ascorbate, 10 mM sodium pyruvate, or 1 mM cystathionine, and 200 μg/mL nanoceria. Intracellular basal ROS levels were evaluated by H_2DCFDA staining at the indicated time points. Values are expressed as fold reduction of the DCF signal with respect to control and are the mean of three independent experiments $\pm$ SD; only nanoceria shows significantly different values between 48 and 72 h (asterisk); *$p < 0.05$ compared to the control.

Figure 4B. These results show that nanoceria reduces apoptosis by interfering with the apoptotic signaling and not with the peculiar type of damage produced by any of the inducers used. Additional means of apoptotic analysis in etoposide-treated U937 confirmed the anti-apoptotic effect of nanoceria: 200 μg/mL nanoceria reduces the abundance of sub-G1 cells (Figure 4C) and cells with low mitochondria membrane potential (Figure 4D); the corresponding increase in cell viability was confirmed by the MTT assay (Figure 4E).

We evaluated the effect of the sedimentation protocol on the anti-apoptotic effect of nanoceria, showing that also in this case the active fraction is limited to the nanoceria remaining in the supernatant (Figure 4F).

Nanoceria also diminishes apoptotic nuclear fragmentation in etoposide-treated Jurkat cells in a dose-dependent fashion and contrasts the decrease in viability due to etoposide treatment (Figure 4G,H).

Nanoceria Completely Prevents Apoptotic ROS Formation. We then investigated the mechanisms of nanoceria anti-apoptotic effect, with the goal of validating the general assumption that the anti-apoptotic action is a consequence of nanoceria antiradical effect. It is known that all apoptotic cells develop ROS at the end of the process because of mitochondrial alterations; but only in some types of apoptosis are ROS and peroxides produced in pre-apoptotic cells.[40] In such instances, the oxidative alterations are an integral part of apoptotic signal transduction, and their inhibition prevents the development of apoptosis.[43,44] Puromycin and etoposide are not direct oxidant agents but induce cells to extrude glutathione (GSH), the main intracellular antioxidant, depleting antioxidant defenses and causing cells to autoproduce an oxidative stress that promotes apoptosis.[45,46] To understand whether nanoceria reduces apoptosis because of its radical scavenging ability, we first evaluated whether nanoceria may scavenge ROS and peroxide produced in pre-apoptotic cells. We found that nanoceria dose-dependently decreased the pre-apoptotic ROS elicited in U937 by etoposide, up to their complete inhibition with the largest dose (the nominal 200 μg/mL) (Figure 5A); this is confirmed by the time course analysis of ROS with the 200 μg/mL dose (Figure 5B). Also, pre-apoptotic superoxide is completely eliminated (Figure 5C), as well as GSH loss (Figure 5D). Also, on Jurkat cells, 200 μg/mL nanoceria prevented pre-apoptotic ROS and superoxide generation (Figure 5E,F).

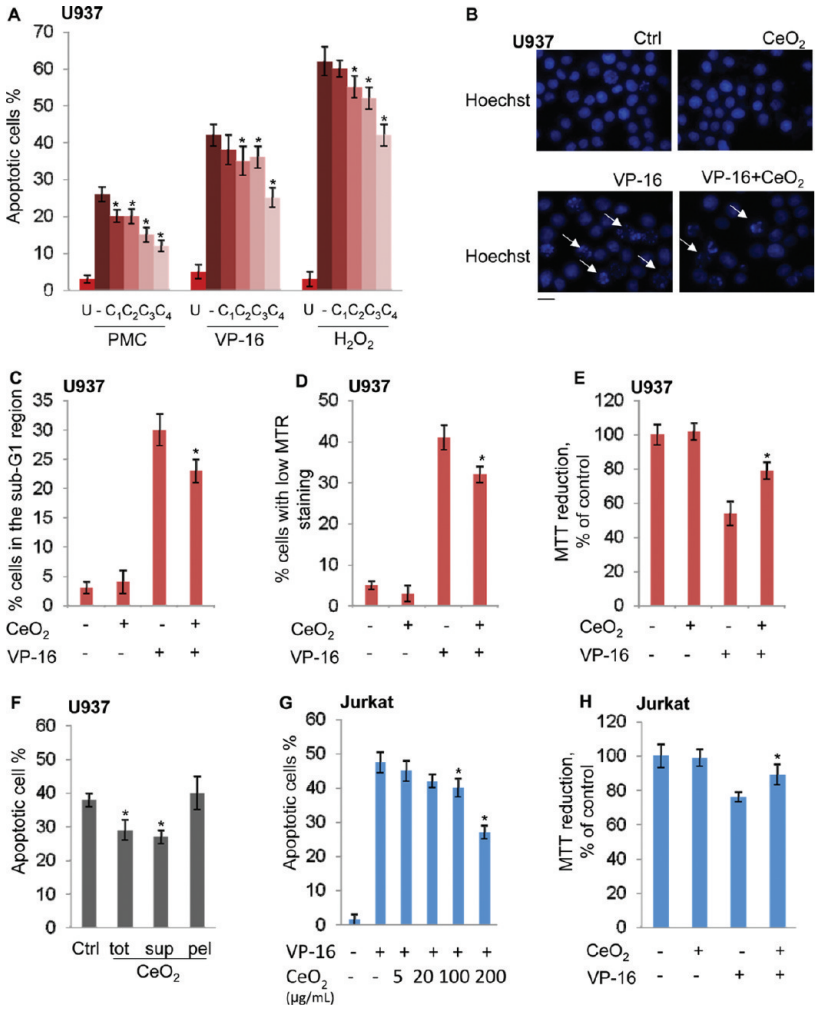

Figure 4. Nanoceria reduces damage-induced apoptosis. (A) Effect of 5, 20, 100, and 200 μg/mL of nanoceria on apoptosis induced by PMC, VP-16, and H_2O_2. U, untreated; −, apoptosis inducer; (C_1−C_4), apoptosis inducer in the presence of 5 (C_1), 20 (C_2), 100 (C_3), and 200 (C_4) μg/mL of nanoceria. Apoptosis values are given as the fraction of apoptotic nuclei after 150 min (VP-16), 240 min (PMC), or 18 h of recovery from H_2O_2 and are the mean of four independent experiments ± SD; *p < 0.01 compared to the apoptosis inducer alone. (B) Fluorescence microscopy images of Hoechst-stained U937 cells ± VP-16 (150 min) ± 200 μg/mL nanoceria (210 min), as indicated. White arrows indicate apoptotic cells; bar = 20 μm. (C) Fraction of U937 cells with sub-G1 DNA content (PI staining) after treatment with VP-16 ± 200 μg/mL nanoceria. (D) Fraction of U937 cells with low mitochondrial membrane potential (MTR staining) after treatment with VP-16 ± 200 μg/mL nanoceria; *p < 0.01 compared to the etoposide alone. Results in C and D show fold increase with respect to control and are the average of three independent experiments ± SD; *p < 0.01 compared to the etoposide alone. (E) U937 cell viability after 150 min of VP-16 ± 200 μg/mL nanoceria, evaluated by the MTT assay; results indicate % variation with respect to control and are the average of four independent experiments ± SD; *p < 0.05 compared to etoposide treatment. (F) Apoptosis induced by VP-16 showed that super fraction of nanoceria retained all of the anti-apoptotic effect of nanoceria and are the average of three independent experiments ± SD. (G) Effect of 5, 20, 100, and 200 μg/mL of nanoceria on VP-16-induced apoptosis on Jurkat cells; apoptosis values are given as the fraction of apoptotic nuclei at 180 min of VP-16 and are the average of three independent experiments ± SD; *p < 0.01 compared to etoposide alone. (H) Jurkat cell viability after 180 min of VP-16 ± 200 μg/mL nanoceria, evaluated by the MTT assay; results indicate % variation with respect to control and are the average of four independent experiments ± SD; *p < 0.01 compared to etoposide treatment.

Nanoceria Selectively Inhibit Redox-Dependent Apoptosis. Overall, the 200 μg/mL nanoceria dose completely abolishes the preapoptotic oxidative alterations of etoposide; however, it only partially prevents apoptosis. To explain this discrepancy, we considered that etoposide triggers two different, independent apoptotic routes in U937 cells, characterized by different redox features[42] and requirements,[43,45] occurring stochastically in the cell population; we hypothesized that nanoceria may affect only the redox-dependent apoptotic pathway. To prove this assumption, we exploited the notion that the two routes display different types of nuclear fragmentation,[47] easily recognizable after nuclear staining, namely, the *cleavage* and the *budding* types. To confirm the link between oxidation and apoptotic nuclear morphology, we performed the following double-labeling experiments. Figure 6A shows the fluorescence microscopy analysis of cells double-labeled with Hoechst to identify the nuclear morphology (top) and with the GSH-specific dye

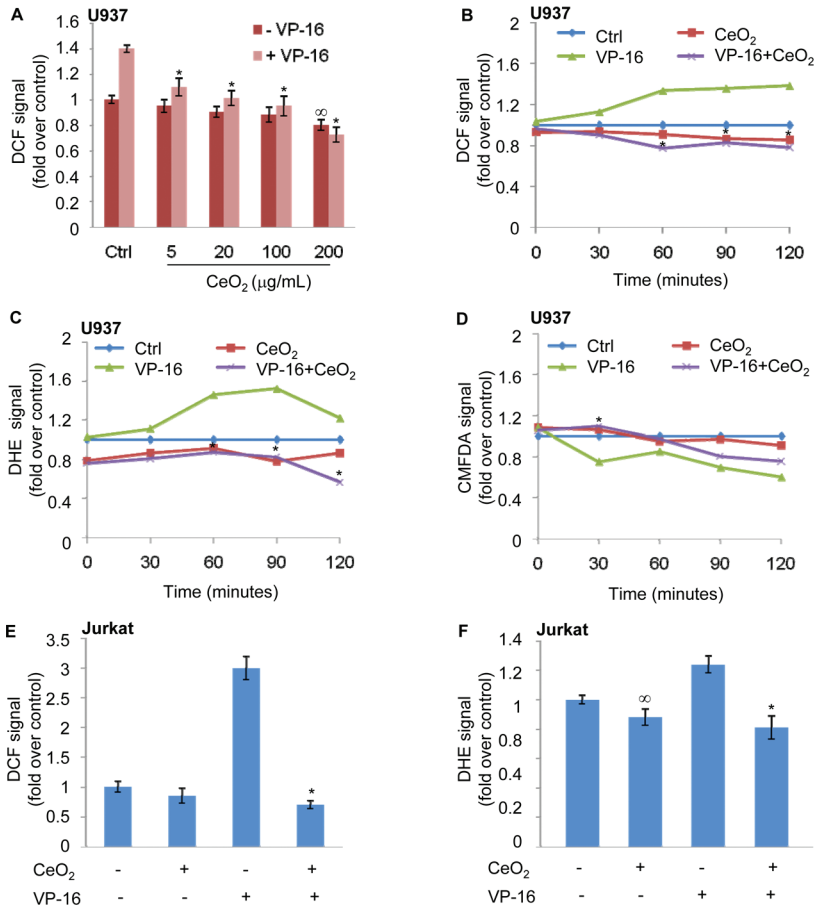

Figure 5. Nanoceria prevents apoptotic redox imbalance. Effect of nanoceria on intracellular ROS induced by VP-16 treatment: (A) comparison of the effect of nanoceria (5, 20, 100, and 200 μg/mL) on DCF signal of U937 cells in the presence/absence of VP-16 (150 min, after 1 h pretreatment with nanoceria); results are expressed as fold reduction over control and are the average of four independent experiments $\pm$ SD; *$p < 0.05$ compared to etoposide alone; $\infty p < 0.01$ compared to the control alone. Time course analysis of intracellular apoptotic ROS (B), apoptotic superoxide (C), and GSH content (D), evaluated on U937 at different times of VP-16 after 1 h of preincubation with 200 μg/mL nanoceria. Values indicate fold increase with respect to control and are each the mean of three independent experiments with similar results; the asterisks indicate time points where values of VP16 + nanoceria significantly differ from VP16 alone; *$p < 0.01$. Effect of 1 h pretreatment with 200 μg/mL nanoceria on intracellular ROS (E, DCF signal) and superoxides (F, DHE signal) produced on Jurkat cells at 150 min of VP-16 treatment. Values indicate fold increase with respect to control. Results are the average of four independent experiments $\pm$ SD; *$p < 0.01$ compared to the etoposide alone; $\infty p < 0.01$ compared to the control alone.

chloromethylfluorescein diacetate (CMFDA) to evaluate intracellular GSH levels (bottom): cleavage is associated with low GSH staining, indicating proneness to oxidative stress, whereas budding cells have a GSH content similar to viable cells (Figure 6B; see also ref 42). To further analyze the oxidative features of apoptotic cells in cleavage *versus* budding, we performed a double labeling (see Figure 6B) with Hoechst (top) and the ROS dye dihydrodichlorofluorescein diacetate (H_2DCFDA, bottom): in budding cells, the dichlorofluorescein (DCF) signal is similar to viable cells, whereas cells in cleavage show stronger staining, indicating an oxidative status. Since no exception to this behavior was found examining >300 cells in more than five independent experiments for any of the double-labeling experiments, these analyses show that only cleavage develops oxidative alterations, and that the nuclear apoptotic morphology is a reliable marker allowing distinguishing between redox-dependent *versus* independent apoptosis. At this point, we evaluated the effect of nanoceria on the abundance of the two apoptotic morphologies; the results are shown in Figure 6C. Nanoceria strongly contrasts the cleavage morphology, up to the point of inverting the frequency ratio between the two morphologies with respect to etoposide alone (Figure 6C). Interestingly, nanoceria behaves exactly like the antioxidant agent cystathionine, which exerts partial reduction of apoptosis,[45] complete abolishment of oxidative alterations,[43] and prevention of the cleavage morphology[42] (Figure 6C; complete shift of all apoptotic cells to budding). Co-treatment of cystathionine plus nanoceria does not further affect the system, suggesting that the two treatments act on the same target.

Glutathione is actively extruded in the reduced form (GSH) from the apoptosing cells,[45,46] promoting the oxidative dimerization and mitochondrial translocation

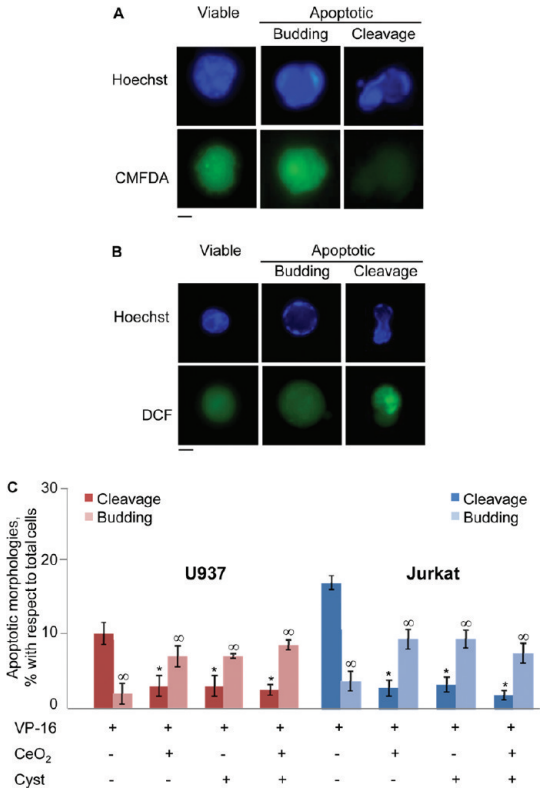

Figure 6. Nanoceria inhibits only oxidation-dependent apoptosis. Micrographs of U937 cells untreated or induced to apoptosis, double-labeled with Hoechst (A,B, top; nuclear morphology) and CMF (A, bottom; GSH content), or DCF (B, bottom; ROS content). For A and B (left), viable cell; (center) apoptotic cell in budding; (right) apoptotic cell in cleavage; bars =10 μm. Budding cells always (>300 cells examined) show normal (*i.e.*, equal to control) GSH and ROS levels, whereas cells in cleavage always (>300 cells examined) show altered oxidative parameters (low GSH and high ROS). (C) Frequency of the apoptotic morphologies of budding and cleavage among U937 (left) or Jurkat (right) cells induced to apoptosis by VP-16 after pretreatment with 200 μg/mL nanoceria and/or cystathionine (cyst) for 1 h. Cleavage and budding frequencies among total cells were evaluated by Hoechst staining after 120 min (U937) or 150 min (Jurkat) of VP-16. Values are the average of four independent experiments ± SD; *$p < 0.05$ compared to the cleavage in etoposide alone; ∞$p < 0.05$ compared to the budding in etoposide alone.

of Bax[48] and cytochrome *c* release.[40] Cystathionine is an inhibitor of the plasma membrane GSH transporters,[49] which blocks GSH efflux in many instances including apoptosis; this decreases the extent of apoptosis by selectively preventing the cleavage route.[42] Interestingly, plasma membrane GSH transporters are redox-sensitive,[50] thus possibly being a sensible target for the antioxidant effect of nanoceria in apoptosis. That nanoceria mimics cystathionine is suggestive of an extracellular role of nanoceria in the vicinity of plasma membrane and is in agreement with the finding that nanoceria is not internalized according to flow cytometric side scatter measurements (Figure 1B).

Also, Jurkat cells display the two apoptotic morphologies, which are affected in the same way as U937 cells by cystathionine and nanoceria (Figure 6C, right). These results show for the first time a cause–effect relationship between nanoceria antiradical and anti-apoptotic effect.

Antioxidant and Anti-apoptotic Effects of Nanoceria Correlate with the Amount of Ce^{3+} Ions and Not with Oxygen Vacancies. The antioxidant role played by nanoceria in biological systems still requires a precise description in chemical terms. Both the Ce^{3+}/Ce^{4+} redox couple and the oxygen vacancies could account for the biological antioxidant properties, but no analysis aimed at attributing such effects to one or the other features of nanoceria was performed so far, to the best of our knowledge. We took advantage of the possibility of altering Ce^{3+}/Ce^{4+} ratio without affecting oxygen vacancies by doping nanoceria with a second rare earth element, samarium, which has a 3+ oxidation state. Sm-doped ceria is already used for solid oxide fuel cell electrolytes[17,51] because Sm doping reduces electronic conductivity caused by the presence of Ce^{3+}/Ce^{4+} couples that allows polaron hopping and increases ionic conductivity (up to a Sm content of 20 at %) owing to an increase in oxygen vacancy concentration. We synthesized nanosized Sm-doped ceria (SDC) powders,[17] heating to 450 °C with Sm concentrations of 5, 10, and 20 at % with respect to cerium, without affecting the oxygen vacancy content due to the presence of Ce^{3+} in the nanosized particles. XPS analysis, performed to measure the Ce^{3+}/Ce^{4+} ratio, showed a progressive decrease in Ce^{3+} concentration (Figure 7A; for details, see Supporting Information I, Figures S1 and S2). The TEM analysis showed that the mean grain size slightly increased up to 15 nm with increasing the Sm content (see Supporting Information II, Figure S3), in agreement with crystallite size measurements from XRD analysis (see Supporting Information SII). The XRD analysis of the powders showed a single fluorite phase for all the samples (see Supporting Information II, Figure S4).

These materials were analyzed for the *in vitro* antiradical properties and their biological effects on intracellular ROS and apoptosis. Sm doping dose-dependently blunts the effects of nanoceria in terms of galvinoxyl reduction (Figure 7B), of intracellular basal (Figure 7C) and apoptotic (Figure 7D) ROS scavenging, and in terms of the anti-apoptotic (Figure 7E) and prosurvival (Figure 7F) effects; similar results were found on Jurkat cells (see Figure S5 in Supporting InformationS5). Interestingly, the 20 at % Sm-doped nanoceria showed, for all of the parameters tested, values resembling those obtained in the absence of nanoceria. This evidence shows that the antioxidant and anti-apoptotic effects of nanoceria correlate with the fraction of Ce^{3+} atoms and not with oxygen vacancies. In principle, other features of the doped nanoparticles may influence the results. To approach this issue, we considered the physicochemical characteristics of the doped nanoparticles, which are listed in

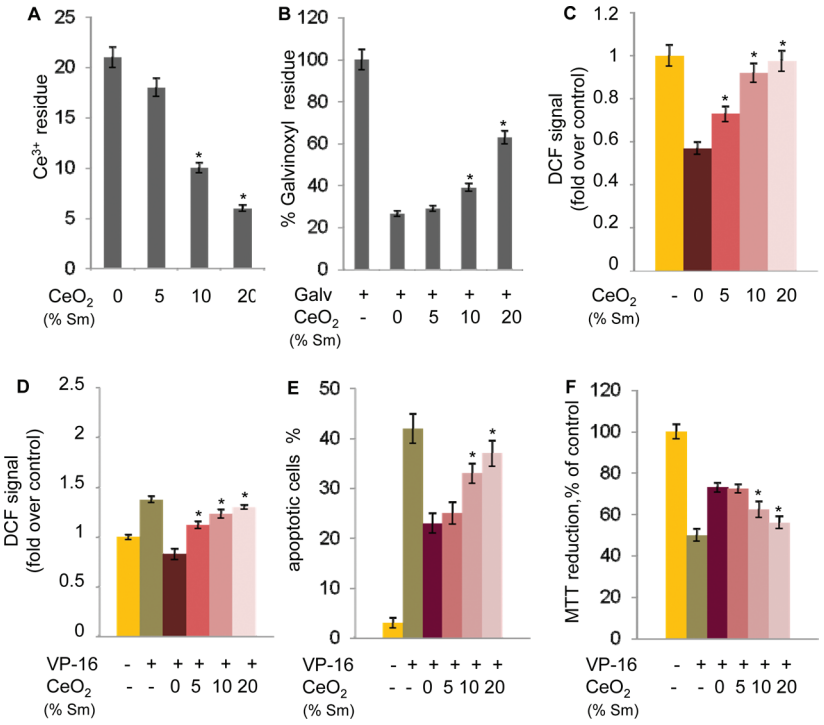

Figure 7. Samarium doping prevents the effects of nanoceria. (A) Ce^{3+} content in undoped and Sm-doped nanoceria, as assessed by XPS; 0, 5, 10, and 20 indicate the at % of Sm doping. Values are the average of three independent measurements ± SD. (B) Galvinoxyl (100 μM) reduction by plain or Sm-doped nanoceria (100 μg/mL) evaluated after 2 h of incubation. 0, 5, 10, and 20 indicate the Sm doping at % concentration. Values are given as the % reduction of galvinoxyl and are the average of four independent experiments ± SD. Intracellular (C) basal ROS levels (measured at 24 h of incubation) and (D) apoptotic ROS levels (measured at 90 min of VP-16), after incubation with undoped or doped nanoceria. Nanoceria preparations were used at 200 μg/mL; 0, 5, 10, and 20 indicate the Sm doping at % concentration. Results indicate fold increase with respect to control. Values are the average of four independent experiments ± SD. (E) Apoptosis evaluated as the fraction of apoptotic nuclei after 1 h preincubation with undoped or doped nanoceria (200 μg/mL) followed by 150 min of etoposide. (F) Cell viability measured as MTT assay in the same conditions as in E. Results indicate fold increase with respect to control. Values are the average of four independent experiments ± SD; (A–F) *p < 0.05 compared to undoped nanoceria.

TABLE 1. Summary of the Main Physical–Chemical Properties of the Nanoceria Preparations (Undoped and Doped), Quantitatively Comparing the Main Activities as Antioxidant and Anti-apoptotic Agents[a]

					antioxidant					
	features				*in vitro*		in cells		anti-apoptotic	
particle	size (nm)	SSA (m^2/g)	zeta-potential at pH 7 (eV)	% Ce^{3+}	protection (% of control)	activity/SSA	protection (% of control)	activity/SSA	protection (% of control)	activity/SSA
nanoceria	6	57	−27.6	21	73	1.28	45	0.78	46	0.80
nanoceria w/ 5% Sm	10	58	−27.2	18	71	1.22	32	0.55	41	0.70
nanoceria w/ 10% Sm	11	63	−26.5	10	61	0.97	13	0.20	22	0.34
nanoceria w/ 20% Sm	13	47	−25.9	6	37	0.78	5	0.10	12	0.25

[a] Values for each parameter are given as % decrease (protection) with respect to control. Normalization per specific surface area (SSA) does not substantially alter any of the activities.

Table 1 together with the quantification of the antioxidant effects. Measurements of zeta-potential were performed on the different powders to determine whether Sm doping may change surface chemistry, resulting in different interactions with cells. The powders displayed negative charges at all of the pH values investigated, as a fingerprint of the basic synthesis method. The zeta-potential did not significantly change with increasing the Sm concentration (Table 1), excluding its influence on biological interactions. The increase in size due to doping is not influent because normalization of all the results per surface area of the doped nanoparticles does not substantially change the results (Table 1). We also excluded that Sm doping decreases the fraction of nanoparticles left in the colloidal, active phase after sedimentation in

water, which was about 10% of the total mass, for doped and undoped nanoceria alike. In addition, we ruled out the possibility that Sm doping was simply "diluting" Ce, because (a) Sm substitution as low as 20% totally reverted the biological effects of nanoceria; (b) pure Sm oxide nanoparticles showed effects of their own that were not observed when Sm is present as doping material (preliminary observations). All of these findings convey to ascribe the anti-apoptotic effect of nanoceria to the concentration of Ce^{3+} ions. This does not exclude that oxygen vacancies may interfere with other types of biological signaling. Indeed, doping nanoceria with Er, a lanthanide resembling Sm in terms of valence and redox reactivity, failed to impair the scavenging activity of nanoceria against H_2O_2,[52] an effect that was attributed to oxygen vacancies rather than to Ce^{3+} ions.

CONCLUSIONS

With this study, we meant to begin building a bridge between the analytical studies about the chemical antioxidant mechanisms of nanoceria and the accumulating observation studies about their roles in biological systems.

On the one side, tailoring the materials properties allowed performing a mechanistic analysis on nanoceria effect on living matter. The defect type and concentration was tailored through Sm doping, which decreases Ce^{3+} without affecting the oxygen vacancy contents. The finding that samarium doping progressively deprives nanoceria of its antioxidant and anti-apoptotic abilities allows establishing that oxygen vacancies do not contribute to the cellular antioxidant and anti-apoptotic effects of nanoceria, which are instead correlated to the presence of Ce^{3+} ions. Such findings provide strong support to the hypothesis that Ce^{3+}/Ce^{4+} redox reactions are responsible for the outstanding biological properties of nanoceria.

On the other side, the characterization of redox-dependent and independent apoptosis provided a novel tool to determine the mechanism of the anti-apoptotic effect of nanoceria, demonstrating that nanoceria only affects the redox-dependent apoptosis and establishing a direct cause–effect relationship between the cell antiradical and prosurvival effects of nanoceria.

Understanding the mechanism of the biological effects of nanoceria will help focusing its potential pharmacological use in consideration of clinical trials concerning antioxidant therapy.

MATERIALS AND METHODS

Preparation and Characterization of Ceramic Nanopowders. Nanostructured oxide powders were synthesized through a wet-chemical process at room temperature. The synthesis procedure is reported in detail in previous papers for the undoped[36] and the Sm-doped nanoceria, $Ce_{1-x}Sm_xO_{2-0.5x-\delta}$ (SDC).[17] Three different compositions for Sm content were here investigated: $x = 0.05$, 0.10, and 0.20. The nanotitania powders were prepared according to the procedure described elsewhere.[53] Phase and morphology of the produced nanopowders were characterized using X-ray diffractometer (XRD, X'pert 1900, Philips) and high-resolution transmission electron microscope (HR-TEM, JEM-F2100, JEOL) operated at an acceleration voltage of 200 kV, respectively. Specific surface area measurements were conducted on the powders using BET analysis (AUTOSORB-1, Quantachrome Instruments).

Materials. Hoechst 33342, etoposide (VP-16), propidium iodide (PI), 3-(4,5-dimethylthiazol-2-yl)-2,5-diphenyltetrazolium (MTT), puromycin (PMC), hydrogen peroxide (H_2O_2), galvinoxyl and cystathionine (cyst), sodium pyruvate, trolox, and sodium ascorbate were purchased from Sigma-Aldrich Corp., St. Louis, MO, USA. MTR, H_2DCFDA, DHE, and CMFDA were purchased from Molecular Probes, Invitrogen, Italy. Stock solutions: Hoechst 33342 (10 mg/mL), sodium pyruvate (10 mM), and sodium ascorbate (100 μM) were dissolved in distilled water; etoposide (50 μM), MTR (1 mM), CMFDA (1 mM), H_2DCFDA (10 mM), and DHE (10 mM) were dissolved in DMSO; galvinoxyl (5 mM) was dissolved in methanol; cystathionine (10 mM) was dissolved in RPMI 1640; trolox (250 mM), PI (5 mg/mL), MTT (5 mg/mL), and PMC (10 mg/mL) were dissolved in sterile PBS.

Nanoceria Suspensions. Nanoceria powders were suspended in deionized distilled water at the concentration of 1 or 10 mg/mL, sonicated for 5 min at 30% amplitude (Branson Ultrasonic Corp., Danbury, CT, USA), vortexed for 20 min, and immediately added to the culture medium. The experiments were performed adding cerium oxide nanoparticles to the culture medium at the nominal concentrations of 5, 20, 100, and 200 μg/mL. To separate the supernatant fraction, 10 mg of nanoceria was suspended in H_2O, sonicated as described, and let to sediment by gravity for 18 h at 4 °C. Eight hundred microliters of supernatant was pipetted and vacuum-dried; the powder was weighed and characterized by TEM, as described above. For the biological tests, the original 800 μL volume was reconstituted with H_2O and used in parallel with total nanoceria, together with rehydrated sedimented fraction. For zeta-potential measurements, the powders were suspended as described above in deionized distilled water buffered at different pH values. Measurements were performed using a LEZA-600 laser zeta-potential analyzer (Otsuka Electronics. Co., Japan) and using ELS-8000 software package (supplied by the same manufacturer) for data visualization and analysis. The pH values investigated were 3 (40.8% v/v HCl/C_6H_4(COOK)(COOH)), 7 (59.4% v/v NaOH/KH_2PO_4), and 9 (42.6% v/v NaOH/KCl+H_3BO_3 solution). All reagents were purchased by Sigma-Aldrich (USA) and dissolved in bidistilled water to obtain 0.2 M solutions. Adjustments of the pH were performed when necessary by controlled addition of HCl or NaOH.

Electron Paramagnetic Resonance Spectroscopy Measurements. A galvinoxyl stock solution (5 mM in ethanol 95%) was freshly prepared immediately before the experiments, as described elsewhere.[54] Tests were performed with galvinoxyl solutions as a control and on nanoceria suspensions. Nanoceria preparations were incubated in galvinoxyl solutions (10 or 100 μM as described in the figure legends) for 2 h at room temperature. The suspensions were drawn into glass capillaries, sealed, and measured using an ESP300 instrument (Bruker Spectrospin, Karlsruhe, Germany) equipped with a high-sensitivity TM_{110} X-band cavity. Radical spectra were recorded at room temperature, using 0.6 G modulation, 1 mW microwave power, and a scan time of 42 s for a 30 G spectrum. Normally, four spectra were accumulated for each measurement to obtain a suitable signal-to-noise ratio. The kinetics of the reaction was followed for 3 h at room temperature or until the radical signal had disappeared.

Cell Culture. U937 cells, human tumor monocytes,[55] and Jurkat cells, human tumor T lymphocytes,[56] were grown at

37 °C in RPMI 1640 medium supplemented with 10% fetal bovine serum (FCS), 2 mM L-glutamine, 100 IU/mL penicillin and streptomycin, in a humidified atmosphere of 5% CO_2 in air. All experiments were performed on cells in the logarithmic phase of growth under condition of ≥98% viability. Cells were kept at the concentration of 10^6/mL.

Flow Cytometric Detection of Forward and Side Scatter. Cells were incubated for 2.5 h with 100 μg/mL nanoceria or nanotitania; forward and side scatter was evaluated by FACSCalibur flow cytometer, and data were analyzed with WinMdi 2.9 software.

Antioxidant Treatments. U937 cells were incubated at 37 °C for up to 72 h with either 1 mM trolox, 100 μM sodium ascorbate, 10 mM sodium pyruvate, 1 mM cystathionine, or 200 μg/mL nanoceria. Intracellular basal ROS levels were evaluated by H_2DCFDA staining at the indicated time points.

Induction and Evaluation of Apoptosis. Apoptosis was induced by the following agents:

(i) 10 μg/mL puromycin, a protein synthesis inhibitor that causes premature chain termination by acting as an analog of the 3′-terminal end of aminoacyl-tRNA. PMC was kept throughout the experiment; nanoceria was added 60 min prior to PMC.

(ii) 1 mM hydrogen peroxide, added to medium culture for 1 h; cells were washed and placed in fresh medium for recovery to allow apoptosis development; nanoceria was added during recovery to avoid possible scavenging of H_2O_2 due to the antioxidant ability of nanoceria.

(iii) 100 μM etoposide, a topoisomerase II inhibitor inducing apoptosis *via* DNA damage. VP-16 was kept throughout the experiment; nanoceria was added 60 min prior to VP-16.

Apoptosis was quantified as follows:

(a) Fraction of apoptotic nuclei. Apoptotic cells fragment their nuclei in vesicles easily recognizable after DNA staining at the fluorescent microscopy.[57] The fraction of apoptotic nuclei among the total cell population was calculated by counting at the fluorescence microscope at least 300 cells in at least three independent randomly selected microscopic fields, after staining cells with the cell-permeable DNA-specific dye Hoechst 33342 directly added to the culture medium at the final concentration of 10 μg/mL.

(b) Sub-G1 apoptotic peak: apoptotic cells fragment their DNA that exit cells after membrane permeabilization, thus decreasing intracellular content to a sub-G1 level (*i.e.*, lower than cells before DNA replication), detectable upon flow cytometric analysis after staining with the DNA-specific dye propidium iodide;[56] 10^6 cells were centrifuged at 800 rpm for 5 min, resuspended in 100 μL methanol/acetone (4:1), and incubated at 4 °C for 40 min. Then, 500 μL of 100 μg/mL PI were added and incubated at room temperature for 20 min. Cells were analyzed by FACSCalibur flow cytometer, and data were analyzed with WinMdi 2.9 software. Cells falling in the sub-G1 region are considered as apoptotic.

(c) Mitochondrial transmembrane potential. In apoptosis, mitochondria lose their membrane potential, phenomenon that can be detected with sensitive probes and quantified by flow cytometry.[58] MitoTracker Red (MTR) CMXRos (used as 100 nM, excitation 579 nm/emission 599 nm) is a red fluorescent dye that stains active mitochondria according to their membrane potential. MTR is applied to cells and kept at 37 °C for 30 min. Mitochondria membrane potential was evaluated by FACSCalibur flow cytometer, and data were analyzed with WinMdi 2.9 software.

Cell Viability. Cell viability was evaluated by MTT assay; yellow MTT is reduced to purple formazan in the mitochondria of living cells only when mitochondrial reductase enzymes are active. After the treatments, 100 μL cell suspension was transferred in 96-well plates, and 10 mL of MTT (5 μg/mL) was added and incubated at 37 °C for 1 h. At the end of the incubation period, the converted dye is solubilized with 100 μL of acidic isopropyl alcohol (0.04 M HCl in absolute isopropyl alcohol) by thorough pipetting. Absorbance of the converted dye is measured at a wavelength of 570 nm by Benchmark microplate reader (Biorad). Nanoceria slightly affected the MTT assay only at 200 μg/mL concentration, where it increased the absorbance values of <10%.

Detection and Quantification of Intracellular ROS, Superoxide, and Glutathione. Reactive oxygen species were measured by 10 μM dihydro 2′,7′-dichlorofluorescin diacetate (H_2DCFDA, excitation 492 nm/emission 517 nm), a cell-permeable dye that fluoresces only when de-exterified and oxidized to dichlorofluorescein (DCF) by a set of intracellular ROS, thus allowing their quantitative assessment. Superoxide production was assayed using 5 mM dihydroethidium (DHE, excitation 370 nm/emission 420 nm), which is sensitive to oxidation by superoxide. Intracellular glutathione (GSH) content was detected by staining with the specific dye 5-chloromethylfluorescein diacetate (CMFDA, excitation 492 nm/emission 517 nm; used at 10 nM). H_2DCFDA and DHE were added directly to the cell samples, whereas CMFDA requires resuspending cells in serum-free medium. All of the probes were incubated at 37 °C in the dark for 20 min; then cells were analyzed by FACSCalibur flow cytometer; data were analyzed with WinMdi 2.9 software; the mean values were used for tables and graphs. Alternatively, stained cells were observed at the fluorescence microscope.

Statistical Analysis. Data are presented as means ± SD. Statistical evaluation was conducted by a one-way ANOVA, followed by Tukey's Multiple Comparison Test. Statistical significance was set at $p < 0.05$.

Acknowledgment. This work was supported in part by the 2008 PRIN project "miRNA in diagnosis and experimental therapy *via* nano-vectors of pleural malignant mesothelioma" of the Italian Ministry of Education, University and Research (MIUR), and by the World Premier International Research Center Initiative of MEXT, Japan.

Supporting Information Available: (I) XPS analysis of undoped and Sm-doped nanoceria. (II) Structural and morphological analysis of Sm-doped nanoceria powders, and Figure S5 showing that Sm doping prevents the effects of nanoceria on Jurkat cells. This material is available free of charge *via* the Internet at http://pubs.acs.org.

REFERENCES AND NOTES

1. Dröge, W. Free Radicals in the Physiological Control of Cell Function. *Physiol. Rev.* **2002**, *82*, 47–95.
2. Beckman, K. B.; Ames, B. N. Oxidative Decay of DNA. *J. Biol. Chem.* **1997**, *272*, 19633–19636.
3. Halliwell, B. Role of Free Radicals in the Neurodegenerative Diseases: Therapeutic Implications for Radical Theory. *Resp. Physiol.* **2001**, *128*, 379–391.
4. Mashima, R.; Witting, P. K.; Stocker, R. Oxidants and Antioxidants in Atherosclerosis. *Curr. Opin. Lipidol.* **2001**, *12*, 411–418.
5. Aggarwal, B. B.; Sundaram, C.; Prasad, S.; Kannappan, R. Tocotrienols, the Vitamin E of the 21st Century: Its Potential Against Cancer and Other Chronic Diseases. *Biochem. Pharmacol.* **2010**, *80*, 1613–1631.
6. Micke, O.; Schomburg, L.; Buentzel, J.; Kisters, K.; Muecke, R. Selenium in Oncology: From Chemistry to Clinics. *Molecules* **2009**, *14*, 3975–3988.
7. Lü, J. M.; Lin, P. H.; Yao, Q.; Chen, C. Chemical and Molecular Mechanisms of Antioxidants: Experimental Approaches and Model Systems. *J. Cell. Mol. Med.* **2010**, *14*, 840–860.
8. Halliwell, B.; Gutteridge, J. *Free Radicals in Biology and Medicine*, 4th ed.; Oxford University Press: Oxford, 2007.
9. Esch, F.; Fabris, S.; Zhou, L.; Montini, T.; Africh, C.; Fornasiero, P.; Comelli, G.; Rosei, R. Electron Localization Determines Defect Formation on Ceria Substrates. *Science* **2005**, *309*, 752–755.
10. Fronzi, M.; Soon, A.; Delley, B.; Traversa, E.; Stampfl, C. Stability and Morphology of Cerium Oxide Surfaces in an Oxidizing Environment: A First-Principles Investigation. *J. Chem. Phys.* **2009**, *131*, 104701 (16 pp).

11. Spanier, J. E.; Robinson, R. D.; Zheng, F.; Chan, S. W.; Herman, I. Size-Dependent Properties of CeO_{2-y} Nanoparticles as Studied by Raman Scattering. *Phys. Rev. B* **2001**, *64*, 245407 (8 pp).
12. Deshpande, S.; Patil, S.; Kuchibhatla, S. V. N. T.; Seal, S. Size Dependency Variation in Lattice Parameter and Valency States in Nanocrystalline Cerium Oxide. *Appl. Phys. Lett.* **2005**, *87*, 133113 (3 pp).
13. Zhang, F.; Wang, P.; Koberstein, J.; Khalid, S.; Chan, S. W. Cerium Oxidation State in Ceria Nanoparticles Studied with X-ray Photoelectron Spectroscopy and Absorption Near Edge Spectroscopy. *Surf. Sci.* **2004**, *563*, 74–82.
14. Davis, V. T.; Thompson, J. S. Measurement of the Electron Affinity of Cerium. *Phys. Rev. Lett.* **2002**, *88*, 073003 (4 pp).
15. Zheng, X.; Zhang, X.; Wang, X.; Wang, S.; Wu, S. Preparation and Characterization of CuO/CeO_2 Catalysis and Their Applications in Low-Temperature CO Oxidation. *Appl. Catal. A* **2005**, *295*, 142–149.
16. Murray, E. P.; Tsai, T.; Barnett, S. A. A Direct Methane Fuel Cell with a Ceria-Based Anode. *Nature* **1999**, *400*, 649–651.
17. Esposito, V.; Traversa, E. Design of Electroceramics for Solid Oxide Fuel Cell Applications: Playing with Ceria. *J. Am. Ceram. Soc.* **2008**, *91*, 1037–1051.
18. Corma, A.; Atienzar, P.; Garcia, H.; Chane-Ching, J. Y. Hierarchically Mesostructured Doped CeO_2 with Potential for Solar-Cell Use. *Nat. Mater.* **2004**, *3*, 394–397.
19. Izu, N.; Shin, W.; Matsubara, I.; Murayama, N. Development of Resistive Oxygen Sensors Based on Cerium Oxide Thick Film. *J. Electroceram.* **2004**, *13*, 703–706.
20. Chueh, W. C.; Falter, C.; Abbott, M.; Scipio, D.; Furler, P.; Haile, S. M.; Steinfeld, A. High-Flux Solar-Driven Thermochemical Dissociation of CO_2 and H_2O Using Nonstoichiometric Ceria. *Science* **2010**, *330*, 1797–1801.
21. Chen, J.; Patil, S.; Seal, S.; McGinnis, J. F. Rare Earth Nanoparticles Prevent Retinal Degeneration Induced by Intracellular Peroxides. *Nat. Nanotechnol.* **2006**, *1*, 142–150.
22. Singh, N.; Cohen, C. A.; Rzigalinski, B. A. Treatment of Neurodegenerative Disorders with Radical Nanomedicine. *Ann. N.Y. Acad. Sci.* **2007**, *1122*, 219–230.
23. Karakoti, A.; Singh, S.; Dowding, J. M.; Seal, S.; Self, W. T. Redox-Active Radical Scavenging Nanomaterials. *Chem. Soc. Rev.* **2010**, *39*, 4422–4432.
24. Korsvik, C.; Patil, S.; Seal, S.; Self, W. T. Superoxide Dismutase Mimetic Properties Exhibited by Vacancy Engineered Ceria Nanoparticles. *Chem. Commun.* **2007**, *10*, 1056–1058.
25. Pirmohamed, T.; Dowding, J. M.; Singh, S.; Wasserman, B.; Heckert, E. G.; Karakoti, A. S.; King, J. E. S.; Seal, S.; Self, W. T. Nanoceria Exhibit Redox State-Dependent Catalase Mimetic Activity. *Chem. Commun.* **2010**, *46*, 2736–2738.
26. Celardo, I.; Pedersen, J. Z.; Traversa, E.; Ghibelli, L. Pharmacological Potential of Cerium Oxide Nanoparticles. *Nanoscale* **2011**, *3*, 1411–1420.
27. Lin, W.; Huang, Y. W.; Zhou, X. D.; Ma, Y. Toxicity of Cerium Oxide Nanoparticles in Human Lung Cancer Cells. *Int. J. Toxicol.* **2006**, *25*, 451–457.
28. Hirst, S. M.; Karakoti, A. S.; Tyler, R. D.; Sriranganathan, N.; Seal, S.; Reilly, C. M. Anti-inflammatory Properties of Cerium Oxide Nanoparticles. *Small* **2009**, *5*, 2848–2856.
29. Das, M.; Patil, S.; Bhargava, N. J.; Kang, F.; Riedel, L. M.; Seal, S.; Hickman, J. J. Auto-catalytic Ceria Nanoparticles Offer Neuroprotection to Adult Rat Spinal Cord Neurons. *Biomaterials* **2007**, *28*, 1918–1925.
30. Niu, J.; Azfer, A.; Rogers, L. M.; Wang, X.; Kolattukudy, P. E. Cardioprotective Effects of Cerium Oxide Nanoparticles in a Transgenic Murine Model of Cardiomyopathy. *Cardiovasc. Res.* **2007**, *73*, 549–559.
31. Colon, J.; Hsieh, N.; Ferguson, A.; Kupelian, P.; Seal, S.; Jenkins, D. W.; Baker, C. H. Cerium Oxide Nanoparticles Protect Gastrointestinal Epithelium from Radiation-Induced Damage by Reduction of Reactive Oxygen Species and Upregulation of Superoxide Dismutase 2. *Nanomedicine* **2010**, *6*, 698–705.
32. Colon, J.; Herrera, L.; Smith, J.; Patil, S.; Komanski, C.; Kupelian, P.; Seal, S.; Jenkins, D. W.; Baker, C. H. Protection from Radiation-Induced Pneumonitis Using Cerium Oxide Nanoparticles. *Nanomedicine* **2009**, *5*, 225–231.
33. Kerr, J. F.; Winterford, C. M.; Harmon, B. V. Apoptosis. Its Significance in Cancer and Cancer Therapy. *Cancer* **1994**, *73*, 2013–2026.
34. Hinshaw, D. B.; Sklar, L. A.; Bohl, B.; Schraufstatter, I. U.; Hyslop, P. A.; Rossi, M. W.; Spragg, R. G.; Cochrane, C. G. Cytoskeletal and Morphologic Impact of Cellular Oxidant Injury. *Am. J. Pathol.* **1986**, *123*, 454–464.
35. Asimakopoulos, G. Mechanisms of the Systemic Inflammatory Response. *Perfusion* **1999**, *14*, 269–277.
36. Mandoli, C.; Pagliari, F.; Pagliari, S.; Forte, G.; Di Nardo, P.; Licoccia, S.; Traversa, E. Stem Cell Aligned Growth Induced by CeO_2 Nanoparticles in PLGA Scaffolds with Improved Bioactivity for Regenerative Medicine. *Adv. Funct. Mater.* **2010**, *20*, 1617–1624.
37. Busch, W.; Bastian, S.; Trahorsch, U.; Iwe, M.; Kuhnel, D.; Meissner, T.; Springer, A.; Gelinsky, M.; Richter, V.; Ikonomidou, K.; *et al*. Internalisation of Engineered Nanoparticles into Mammalian Cells *In Vitro*: Influence of Cell Type and Particle Properties. *J. Nanopart. Res.* **2011**, *13*, 293–310.
38. Karakoti, A. S.; Singh, S.; Kumar, A.; Malinska, M.; Kuchibhatla, S. V.; Wozniak, K.; Self, W. T.; Seal, S. PEGylated Nanoceria as Radical Scavenger with Tunable Redox Chemistry. *J. Am. Chem. Soc.* **2009**, *131*, 14144–14145.
39. Havenith, R. W.; de Wijs, G. A.; Attema, J. J.; Niermann, N.; Speller, S.; de Groot, R. A. Theoretical Study of the Stable Radicals Galvinoxyl, Azagalvinoxyl and Wurster's Blue Perchlorate in the Solid State. *J. Phys. Chem. A* **2008**, *112*, 7734–7738.
40. Ghibelli, L.; Coppola, S.; Fanelli, C.; Rotilio, G.; Civitareale, P.; Scovassi, A. I.; Ciriolo, M. R. Glutathione Depletion Causes Cytochrome *c* Release Even in the Absence of Cell Commitment to Apoptosis. *FASEB J.* **1999**, *13*, 2031–2036.
41. Colussi, C.; Albertini, M. C.; Coppola, S.; Rovidati, S.; Galli, F.; Ghibelli, L. H_2O_2-Induced Block of Glycolysis as an Active ADP-Ribosylation Reaction Protecting Cells from Apoptosis. *FASEB J.* **2000**, *14*, 2266–2276.
42. De Nicola, M.; Gualandi, G.; Alfonsi, A.; Cerella, C.; D'Alessio, M.; Bergamaschi, A.; Magrini, A.; Ghibelli, L. Different Fates of Intracellular Glutathione Determine Different Modalities of Apoptotic Nuclear Vesiculation. *Biochem. Pharmacol.* **2006**, *72*, 1405–1416.
43. Liuzzi, F.; Fanelli, C.; Ciriolo, M. R.; Cerella, C.; D'Alessio, M.; De Nicola, M.; Magrini, A.; Bergamaschi, A.; Ghibelli, L. Rescue of Cells from Apoptosis by Antioxidants Occurs Downstream from GSH Extrusion. *Ann. N.Y. Acad. Sci.* **2003**, *1010*, 441–445.
44. D'Alessio, M.; Cerella, C.; De Nicola, M.; Bergamaschi, A.; Magrini, A.; Gualandi, G.; Alfonsi, A. M.; Ghibelli, L. Apoptotic GSH Extrusion Is Associated with Free Radical Generation. *Ann. N.Y. Acad. Sci.* **2003**, *1010*, 449–452.
45. Ghibelli, L.; Fanelli, C.; Rotilio, G.; Lafavia, E.; Coppola, S.; Colussi, C.; Civitareale, P.; Ciriolo, M. R. Rescue of Cells from Apoptosis by Inhibition of Active GSH Extrusion. *FASEB J.* **1998**, *12*, 479–486.
46. Ghibelli, L.; Coppola, S.; Rotilio, G.; Lafavia, E.; Maresca., V.; Ciriolo, M. R. Non-oxidative Loss of Glutathione in Apoptosis *via* GSH Extrusion. *Biochem. Biophys. Res. Commun.* **1995**, *216*, 313–320.
47. Dini, L.; Coppola, S.; Ruzittu, M. T.; Ghibelli, L. Multiple Pathways for Apoptotic Nuclear Fragmentation. *Exp. Cell Res.* **1996**, *223*, 340–347.
48. D'Alessio, M.; De Nicola, M.; Coppola, S.; Gualandi, G.; Pugliese, L.; Cerella, C.; Cristofanon, S.; Civitareale, P.; Ciriolo, M. R.; Bergamaschi, A.; *et al*. Oxidative Bax Dimerization Promotes Its Translocation to Mitochondria Independently of Apoptosis. *FASEB J.* **2005**, *19*, 1504–1506.
49. Fernández-Checa, J. C.; García-Ruiz, C.; Colell, A.; Yi, J. R.; Kaplowitz., N. Inhibition of Rat Sinusoidal GSH Transporter by Thioethers: Specificity, Sidedness, and Kinetics. *Am. J. Physiol.* **1996**, *270*, G969–G975.

50. Kuo, M. T. Redox Regulation of Multidrug Resistance in Cancer Chemotherapy: Molecular Mechanisms and Therapeutic Opportunities. *Antiox. Redox Signal.* **2009**, *11*, 99–133.
51. Steele, B. C. H.; Heinzel, A. Materials for Fuel-Cell Technologies. *Nature* **2001**, *414*, 345–352.
52. Woan, K.; Tsai, Y. Y.; Sigmund, W. Synthesis and Characterization of Luminescent Cerium Oxide Nanoparticles. *Nanomedicine* **2010**, *5*, 233–242.
53. Traversa, E.; Di Vona, M. L.; Licoccia, S.; Sacerdoti, M.; Carotta, M. C.; Crema, L.; Martinelli, G. Sol−Gel Processed TiO_2-Based Nano-sized Powders for Use in Thick-Film Gas Sensors for Atmospheric Pollutant Monitoring. *J. Sol−Gel Sci. Technol.* **2001**, *22*, 167–179.
54. Pedersen, J. Z.; Oliveira, C.; Incerpi, S.; Kumar, V.; Fiore, A. M.; De Vito, P.; Prasad, A. K.; Malhotra, S. V.; Parmar, V. S.; Saso, L. Antioxidant Activity of 4-Methylcoumarins. *J. Pharm. Pharmacol.* **2007**, *59*, 1721–1728.
55. Sundström, C.; Nilsson, K. Establishment and Characterization of a Human Histiocytic Lymphoma Cell Line (U-937). *Int. J. Cancer* **1976**, *17*, 565–577.
56. Schneider, U.; Schwenk, H. U.; Bornkamm, G. Characterization of EBV-Genome Negative "Null" and "T" Cell Lines Derived from Children with Acute Lymphoblastic Leukemia and Leukemic Transformed Non-Hodgkin Lymphoma. *Int. J. Cancer* **1977**, *19*, 621–626.
57. Sasaki, D. T.; Dumas, S. E.; Engleman, E. G. Discrimination of Viable and Non-viable Cells Using Propidium Iodide in Two Color Immunofluorescence. *Cytometry* **1987**, *8*, 413–420.
58. Buckman, J. F.; Hernández, H.; Kress, G. J.; Votyakova, T. V.; Pal, S.; Reynolds, I. J. MitoTracker Labeling in Primary Neuronal and Astrocytic Cultures: Influence of Mitochondrial Membrane Potential and Oxidants. *J. Neurosci. Meth.* **2001**, *104*, 165–176.